# Development of a Reconfigurable Multicopter Flight Dynamics Model from Flight Data Using System Identifcation

**Mark J. S. Lopez** Aerospace Engineer
**Mark B. Tischler** Senior Technologist
**Ondrej Juhasz** Aerospace Engineer
Aviation Development Directorate
U.S. Army RDECOM, Aviation & Missile Center
Moffett Field, CA

**Anthony Gong** Research Associate
**Frank C. Sanders** Senior Research Associate
San Jose State University
Ames Research Center
Moffett Field, CA

## ABSTRACT

Multirotor unmanned aerial systems (UAS) are prone to tubulent wind conditions and gust disturbances. Improving gust rejection performance is a critical technology to enable multirotor UAS operations in highly turbulent conditions and has been a recent topic of interest for study. This work is focused on developing flight dynamics models to better understand the flight characteristics of these multirotor aircraft which directly affect their ability to reject gusts and other external disturbances. This paper uses flight data and system identification to develop and validate a reconfigurable multicopter model. A Joint Input-Output system identification method is used to determine contributions from individual motors. The reconfigurable model is used to gain physical insight on the effects of rotor number and spacing on flight dynamic characteristics and gust rejection capability.

## NOTATION

**Symbols**

| | |
|---|---|
| $\boldsymbol{M}$ | Mixing matrix from summed actuator signals to individual actuator signals |
| $\boldsymbol{r}$ | Vector of reference signals in JIO method |
| $\boldsymbol{y}$ | Vector of output signals |
| $\boldsymbol{\delta}_A$ | Vector of actuator signals in JIO method |
| $\boldsymbol{\delta}_F$ | Vector of individual actuator command signals |
| $\boldsymbol{\delta}_{Sum}$ | Vector of summed actuator command signals |

## INTRODUCTION

Multirotor unmanned aerial systems (UAS) are especially prone to gust disturbances. The Aviation Development Directorate (ADD) at Ames Research Center has been working with the Defense Advanced Research Projects Agency (DARPA) under an effort to explore methods for improving gust rejection capabilities in UAS. One part of this effort is developing flight dynamics models to better understand the flight dynamics characteristics of these multirotor aircraft which directly affect their ability to reject gusts and other external disturbances.

Flight dynamics models for multirotor UAS are not sufficiently mature. While physics-based models exist and are well validated and understood for traditional manned-size full-scale rotorcraft, for UAS the model paramters are rarely known accurately (e.g. aerodynamic coefficients) and assumptions that go into these physics-based models may not apply at the UAS scale and have not been well validated. Furthermore, while a physics-based model approach may be appropriate for full-scale rotorcraft, the development and validation cycle of physics-based modeling is currently unable to keep up with the the rapid fly-crash-fix development cycles of UAS.

There is currently much ongoing work to make physics-based models appropriate for multirotor UAS. Bristeau studied the effects of propeller aerodynamics on flight dynamics for a quadrotor UAS (Ref. 1). Russel performed a study on the level of modeling fidelity needed for comprehensive analysis of multirotor UAS (Ref. 2). Most recently Niemiec has taken steps toward a reconfigurable multicopter flight dynamics model based on first principles (Ref. 3).

While the physics-based model approach is continually improving, system identification (Ref. 4) is an effective approach for obtaining accurate multirotor flight dynamics models from flight data that has been used with great success. Wei first used system identification on a quadrotor UAS to obtain a

Presented at the 8th Biennial Autonomous VTOL Technical Meeting, Mesa, AZ, January 29-31, 2019.
Distribution Statement A: Approved for public release; distribution is unlimited.
Disclaimer: thoughts, opinions, and conclusions are those of the authors and do not specifically represent those of the Department of Defense.

bare-airframe model from closed-loop flight-test data (Ref. 5). Juhasz used system identification to obtain a bare-airframe and turbulence models of an Iris+ quadrotor (Ref. 6). Berrios used the identification results from Juhasz in a control system optimization effort that greatly improved the gust rejection capabilities (Ref. 7).

The work presented herein is an approach for a generic, reconfigurable multicopter flight dynamics model, which is developed based on system identified results from flight data.

## SYSTEM IDENTIFICATION

The reconfigurable model is developed based on flight identified models of quad and octocopter vehicles. A hexacopter vehicle was also built and identified. However, the hexacopter was not used in development of the reconfigurable model, it was used only to verify the reconfigurable model. The quad, hexa, and octocopter vehicles were built using common parts. The primary difference among the configurations is the number and location of arms and rotors. Each vehicle has a hub-to-hub diagonal distance of 1.27 meters, with 0.46 meter diameter rotors. The quad, hexa, and octocopter have masses of 6.1, 7.1, and 8.2 kg respectively, and pictures of each vehicle are shown in Fig. 1.

To develop the reconfigurable model with user selectable number and location of rotors, contributions from individual rotors are needed. Due to the way that forces and moments are usually allocated for multicopter control (all motors simultaneously increase or decrease RPM appropriately to obtain the total desired force or moment command), all motor inputs are inhereintly highly correlated. This property of highly correlated inputs is difficult to deal with for traditional system identification methods (Ref. 4). The work presented herein uses a frequency domain system identification approach of Ref. 4, with an extra post-processing step to address the issue of highly correlated inputs: the Joint Input-Output (JIO) methdology with a careful choice of input signals and transformations.

The JIO method was first developed by Akaike (Ref. 8) to address noise. More recently, the JIO method has been used extensively by Gennaretti et al (Ref. 9) and Hersey et al (Ref. 10) to identify inflow models with highly correlated inputs. Knapp et al (Ref. 11) and Berger et al (Refs. 12, 13) also used the JIO method to identify flight dynamics models with highly correlated inputs. The JIO method is used here to obtain frequency responses and state space models where the inputs are the commands for each individual motor. The method used herein is similar to the method demonstrated by Berger (Ref. 13), however there are additional considerations for the purposes of the reconfigurable model.

### System Identification Signals

At this point, it is useful to define the nomenclature that will be used for describing the system identification and JIO methodology. There are 3 general signals that are used in the JIO methodology: the reference, actuator, and output signals.

(a) Quadcopter

(b) Hexacopter

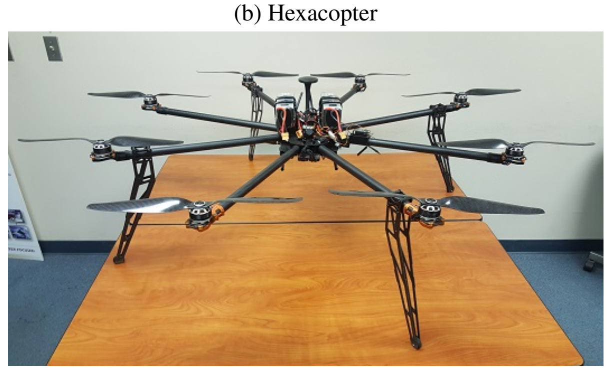

(c) Octocopter

Fig. 1: Pictures of each multirotor vehicle

The output signals $\boldsymbol{y}$ are all rigid body responses of interest and include the standard attitudes and rates in roll, pitch, and yaw ($\phi, \theta, \psi, p, q, r$) in addition to the standard body velocity derivatives and accelerations ($\dot{u}, \dot{v}, \dot{w}, a_x, a_y, a_z$).

The reference signals $\boldsymbol{r}$ are signals used for intermediate frequency response calculations, and are chosen here as the external vehicle commands. For example, during a frequency sweep, the external sweep command is considered as the reference signal; for a vehicle doublet, the external doublet command is considered the reference signal.

The actuator signals $\boldsymbol{\delta}_A$ correspond to the vehicle control effectors, which are the inputs of interest for flight dynamics, but are highly correlated and difficult to use as inputs with traditional system identification methods (Ref. 4). Actuator signals can be individual control effectors (e.g. individual motor commands $\boldsymbol{\delta}_A = \boldsymbol{\delta}_F = [\delta_{F_1}, \delta_{F_2}, ..., \delta_{F_N}]^T$), or alternatively actuator signals can be chosen as pseudo-control effectors (e.g.

sums and differences of motor combinations $\boldsymbol{\delta}_A = \boldsymbol{\delta}_{Sum}$).

Both individual control effectors and pseudo-control effectors are valid choices for actuator signals, and both choices have independent uses. For comparison, a generic block diagram is shown in Fig. 2. In the diagram, $\boldsymbol{P}$ is the bare airframe plant, $\boldsymbol{F}$, $\boldsymbol{C}$, and $\boldsymbol{H}$ are generic flight control blocks, and $\boldsymbol{M}$ is the mixing matrix to convert from summed actuator commands to individual actuator commands. Fig. 2a shows the actuator signals selected as individual motor commands $\boldsymbol{\delta}_A = \boldsymbol{\delta}_F$. Fig. 2b shows the actuator signals selected as summed motor commands $\boldsymbol{\delta}_A = \boldsymbol{\delta}_{Sum}$.

Pseudo-control effectors here are chosen as sums and differences of motor combinations referred to as "summed" actuator commands $\boldsymbol{\delta}_{Sum}$. For a pair of two motors $\delta_{F_i}$ and $\delta_{F_j}$, the summed commands would be symmetric $\delta_{symm} = 1/2(\delta_{F_i} + \delta_{F_j})$ and differential commands $\delta_{diff} = 1/2(\delta_{F_i} - \delta_{F_j})$. For a group of four motors (tetrad), the "summed" actuator commands are chosen as standard $col, lon, lat$ and $ped$ commands which correspond to the four standard decoupled heave, pitch, roll, and yaw commands normally used in flight dynamics and control. The mixing from summed and individual actuator commands is chosen such that mixing matrix is square (number of summed actuator commands is equal to the number of individual actuator commands) and has mutually orthogonal rows and columns; these choices allow the mixing matrix to be invertible so that actuator signals can be easily converted between summed and individual actuator commands.

For a quadcopter with four individual motors ($\boldsymbol{\delta}_F = [\delta_{F_1}, \delta_{F_2}, \delta_{F_3}, \delta_{F_4}]^T$), the four summed actuators are straightforward ($\boldsymbol{\delta}_{Sum} = [col, lon, lat, ped]^T$) and correspond to control of decoupled axes (heave, pitch, roll, yaw). Thus, standard system identifcation methods (Ref. 4) can be used to obtain frequency responses with respect to the four summed actuators with no issues (Ref. 6). The inputs can then be transformed from summed actuators to individual motors, using the mixing matrix $\boldsymbol{M}$, as follows: $\boldsymbol{\delta}_F = [\boldsymbol{M}]\boldsymbol{\delta}_{Sum}$.

For an octocopter with 8 individual motors ($\boldsymbol{\delta}_F = [\delta_{F_1}, \delta_{F_2}, \delta_{F_3}, \delta_{F_4}, \delta_{F_5}, \delta_{F_6}, \delta_{F_7}, \delta_{F_8}]^T$), the 8 motors are divided into 2 groups of 4 (tetrads). As shown in Fig. 3, Tetrad 1 consists of motors 1, 2, 5, and 6, while Tetrad 2 consists of motors 3, 4, 7, and 8. For each octocopter tetrad, the four motors are combined into summed commands $col, lon, lat$ and $ped$. Summed commands for Tetrad 1 are $col_1$ (motors 1, 2, 5, and 6 generate net positive thrust), $lon_1$ (motors 1 and 2 generate more thrust, while 5 and 6 generate less thrust, i.e. net positive pitching moment), $lat_1$ (motors 1 and 6 generate more thrust, while 2 and 5 generate less thrust, i.e. net positive rolling moment), and $ped_1$ (motors 1 and 5 generate more thrust, while 2 and 6 generate less thrust, i.e. net positive yawing moment). Similarly, summed commands for Tetrad 2 are $col_2$ (motors 3, 4, 7, and 8 generate net positive thrust), $lon_2$ (motors 3 and 8 generate more thrust, while 4 and 7 generate less thrust, i.e. net positive pitching moment), $lat_2$ (motors 7 and 8 generate more thrust, while 3 and 4 generate less thrust, i.e. net positive rolling moment), and $ped_2$ (motors 3 and 7 generate more thrust, while 4 and 8 generate less thrust, i.e. net positive yawing moment.). The 8 octocopter summed actuator commands are $\boldsymbol{\delta}_{Sum} = [col_1, lon_1, lat_1, ped_1, col_2, lon_2, lat_2, ped_2]^T$, which are summarized in Table 1 and the summed-to-individual actuator mixing equation given in equation 1.

Table 1: Summed octocopter actuator commands.

| Summed Actuator Command | Description |
|---|---|
| $col_1$ | Tetrad 1 creates net positive heave force |
| $lon_1$ | Tetrad 1 creates net positive pitch moment |
| $lat_1$ | Tetrad 1 creates net positive roll moment |
| $ped_1$ | Tetrad 1 creates net positive yaw moment |
| $col_2$ | Tetrad 2 creates net positive heave force |
| $lon_2$ | Tetrad 2 creates net positive pitch moment |
| $lat_2$ | Tetrad 2 creates net positive roll moment |
| $ped_2$ | Tetrad 2 creates net positive yaw moment |

$$\underbrace{\begin{bmatrix} \delta_{F_1} \\ \delta_{F_2} \\ \delta_{F_3} \\ \delta_{F_4} \\ \delta_{F_5} \\ \delta_{F_6} \\ \delta_{F_7} \\ \delta_{F_8} \end{bmatrix}}_{\boldsymbol{\delta}_F} = \underbrace{\begin{bmatrix} 1 & 1 & 1 & 1 & 0 & 0 & 0 & 0 \\ 1 & 1 & -1 & -1 & 0 & 0 & 0 & 0 \\ 0 & 0 & 0 & 0 & 1 & 1 & -1 & 1 \\ 0 & 0 & 0 & 0 & 1 & -1 & -1 & -1 \\ 1 & -1 & -1 & 1 & 0 & 0 & 0 & 0 \\ 1 & -1 & 1 & -1 & 0 & 0 & 0 & 0 \\ 0 & 0 & 0 & 0 & 1 & -1 & 1 & 1 \\ 0 & 0 & 0 & 0 & 1 & 1 & 1 & -1 \end{bmatrix}}_{\boldsymbol{M}} \underbrace{\begin{bmatrix} col_1 \\ lon_1 \\ lat_1 \\ ped_1 \\ col_2 \\ lon_2 \\ lat_2 \\ ped_2 \end{bmatrix}}_{\boldsymbol{\delta}_{\mathrm{Sum}}} \tag{1}$$

It is important to note that for an octocopter with 4 control channels (heave, pitch, roll ,yaw), the redundancy in summed actuators and control allocation for each channel leads to redundant actuators being fully correlated. Specifically when the vehicle is flown closed loop, pitch channel feedback will be allocated to both $lon_1$ and $lon_2$, meaning that $lon_1$ and $lon_2$ will always be fully correlated. Similarly, roll channel feedback will result in $lat_1$ and $lat_2$ being fully correlated, and yaw channel feedback will result in $ped_1$ and $ped_2$ being fully correlated. Often the heave axis is flown open loop meaning that $col_1$ and $col_2$ can be uncorrelated. The high correlation between redundant summed actuators is addressed using the JIO method.

### Joint Input-Output Method

The system identification goal herein is to determine a bare airframe frequency response matrix $[\boldsymbol{y}/\boldsymbol{\delta}_A]$, where $\boldsymbol{\delta}_A$ are the desired bare airframe inputs or motor commands (actuator signals) and $\boldsymbol{y}$ is the vector of vehicle outputs. Due to the high correlation between bare-airframe inputs, direct identification of the bare airframe frequency response matrix $[\boldsymbol{y}/\boldsymbol{\delta}_A]$ is not possible and the JIO method (Refs. 12, 13) is used instead. The JIO method computes the bare airframe frequency response matrix indirectly by first computing responses with

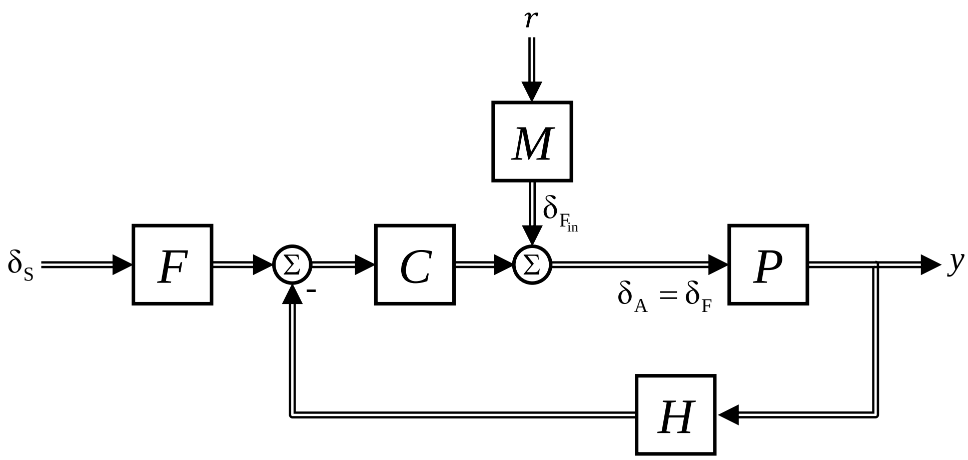


(a) Individual Motor Actuator Signals

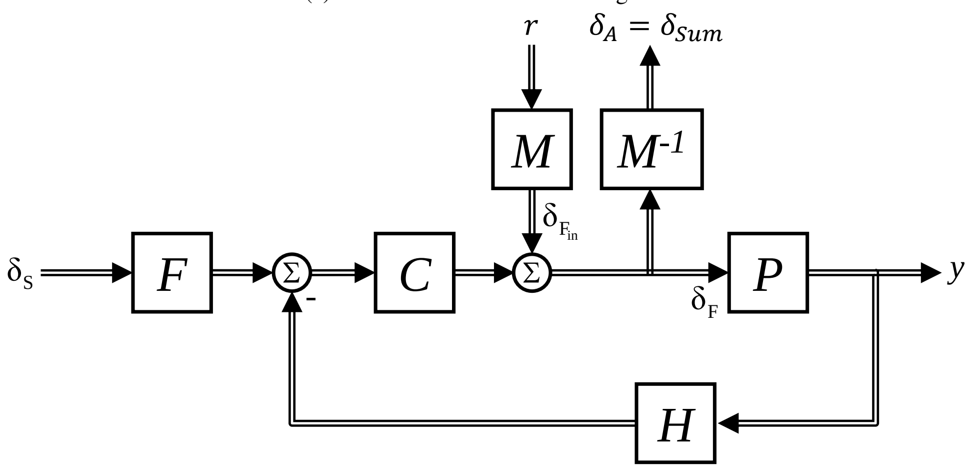


(b) Summed Actuator Signals

Fig. 2: Generic closed-loop block diagram

respect to reference signals $\boldsymbol{r}$, which herein are the external sweep commands. The actuator-to-reference frequency response matrix $[\boldsymbol{\delta}_A/\boldsymbol{r}]$ and output-to-reference frequency response matrix $[\boldsymbol{y}/\boldsymbol{r}]$ are first computed, then at each frequency $\omega$, the bare airframe response matrix is simply the product of the actuator-to-reference frequency response matrix inverse with the output-to-reference frequency response matrix:

$$\left[\frac{\boldsymbol{y}}{\boldsymbol{\delta}_{\mathrm{A}}}(j\omega)\right] = \left[\frac{\boldsymbol{y}}{\boldsymbol{r}}(j\omega)\right]\left[\frac{\boldsymbol{\delta}_{\mathrm{A}}}{\boldsymbol{r}}(j\omega)\right]^{-1} \tag{2}$$

In scalar form, equation 2 can be thought of a simply a chain rule calculation of $y/\delta_A$.

It should be noted that the reference signals are chosen such that they can be independently actuated (and therefore decorrelated) and also that the resulting actuator signals $\boldsymbol{\delta}_A$ are all linearly independent (i.e. that the acutator-to-reference response matrix $[\boldsymbol{\delta}_A/\boldsymbol{r}]$ is square and invertible at all desired frequencies).

For the purposes of obtaining models with individual motor command inputs, there are several considerations when selecting reference signals and actuator signals to process through the JIO method.

The first consideration is with respect to desired responses from external vehicle commands. While one method would be to command frequency exitations to a single individual motor doing so can cause the vehicle to response to be completely coupled between all axes. This can result in responses which have poor signal quality due to the lack of control authority from a single motor. Instead, the vehicle excitations are chosen such that the responses remain decoupled and on-axis as much as possible. Specifically, external vehicle commands are chosen to align closely with the traditional heave, roll, pitch, and yaw commands. For the quadcopter with 4 motors, only 4 vehicle commands are needed and are chosen as the traditional heave, pitch, roll, and yaw commands.

For the octocopter with 8 motors shown in Fig. 3, 8 linearly independent external vehicle commands are needed and are chosen as heave, roll, pitch, and yaw for each tetrad of motors: $\boldsymbol{r} = [col_1, lon_1, lat_1, ped_1, col_2, lon_2, lat_2, ped_2]^T$ as shown in

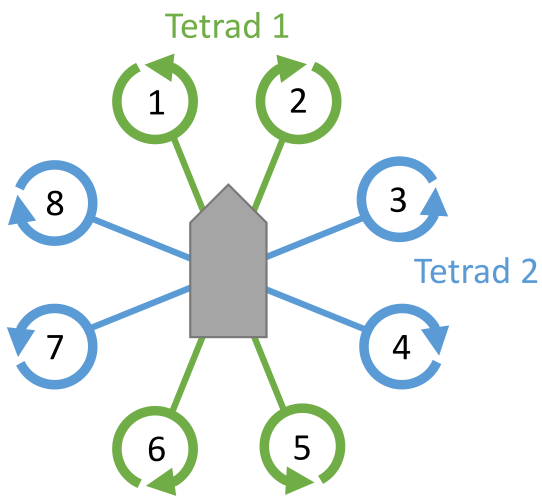


Fig. 3: Octocopter rotor orientations.

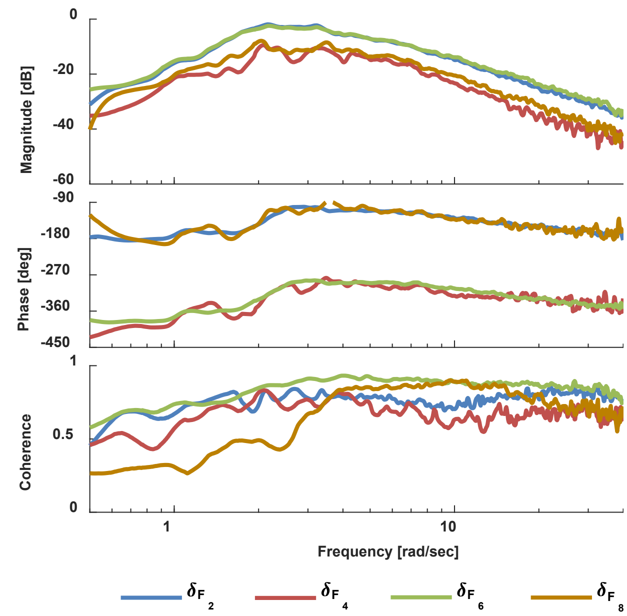


Fig. 4: Octocopter pitch rate response to individual motors $q/\delta_{F_i}$, extracted directly with $\boldsymbol{\delta}_A = \boldsymbol{\delta}_F$.

Table 1. This choice of vehicle commands means that for any particular command, only 2 summed actuator commands are highly correlated for any given frequency sweep excitation. For example, for a pitch sweep command of $lon_1$, only the summed actuator signals $lon_1$ and $lon_2$ will be correlated, with all other summed actuator signals being uncorrelated due to the on-axis nature of the commands. Selection of the vehicle sweep commands and summed actuator signals in this manner means that for any given sweep, only 2 summed actuators need to be considered for the JIO calculation in equation 2. For example, for an octocopter pitch sweep command, one only needs to consider summed actuators $\boldsymbol{\delta}_A = [lon_1, lon_2]^T$; for an octocopter roll sweep command, one only needs to consider summed actuators $\boldsymbol{\delta}_A = [lat_1, lat_2]^T$.

The second consideration is the choice of actuator signals to use in the JIO method. The JIO method can be used to directly obtain frequency responses to individual motors (e.g. $\boldsymbol{\delta}_A = \boldsymbol{\delta}_F$) as illustrated in Fig. 2a. Results for pitch rate response to individual motors is shown in Fig. 4. $\delta_{F_2}$ and $\delta_{F_6}$ have higher control power compared to $\delta_{F_4}$ and $\delta_{F_8}$ as indicated by the higher magnitudes for $\delta_{F_2}$ and $\delta_{F_6}$ above 3 rad/s. The difference in control power in Fig. 4 matches the expected differences based on the rotor placements and differences in moment arms with respect to the vehicle center of gravity.

While Fig. 4 shows that directly obtaining frequency responses to individual motors is possible (e.g. $\boldsymbol{\delta}_A = \boldsymbol{\delta}_F$), there are also variations between the smoothness of responses and therefore overall data quality (e.g., pitch rate $q/\delta_{F_2}$ and $q/\delta_{F_6}$ have much smoother magnitude and phase responses compared to $q/\delta_{F_4}$ and $/q\delta_{F_8}$). It was found that obtaining frequency responses with the summed actuator signals as inputs (e.g. $\boldsymbol{\delta}_A = \boldsymbol{\delta}_{Sum}$) yielded the best coherence and frequency response quality. The reason for this is that vehicle excitation commands were chosen to be heave, pitch, roll, or yaw commands, which are all directly correlated to summed actuator commands in each axis. For example, for a pitch sweep command, individual motors $\boldsymbol{\delta}_F$ will be correlated with the pitch sweep command, but will also be correlated with any off axis responses due to disturbances (e.g. roll feedback to a roll disturbance will be allocated to all individual motors); in contrast, summed actuator commands $lon_1$ and $lon_2$ will be correlated with the pitch sweep command, but will be uncorrelated with any off-axis disturbances (e.g. roll feedback and yaw feedback to disturbances are not allocated to $lon_1$ and $lon_2$) due to the decoupled nature of summed actuator inputs.

**System Identification Process**

The full process is for obtaining models with individual actuators is shown in Fig. 5. The description of each step is shown on the left, and an example for the octocopter in pitch is shown on the right.

The first step is to sweep each reference command $\boldsymbol{r}_i$. In this case, the reference command sweeps $\boldsymbol{r}_i$ are mixed into sweeps of all individual actuators $\boldsymbol{\delta}_{F_{in}}$ as shown in Fig. 2b. In the diagram, $\boldsymbol{M}$ is the mixing matrix to convert from summed actuator commands to individual actuator commands. The individual actuator commands (i.e. commands to each motor $\boldsymbol{\delta}_F = [\delta_{F_1}, \delta_{F_2}, ..., \delta_{F_N}]^T$ are fully correlated. The summed actuator commands $\boldsymbol{\delta}_{Sum}$ are computed by multiplying total individual actuator commands $\boldsymbol{\delta}_F$ with the mixing matrix inverse. Any redundant summed actuator commands will also be fully correlated; for example, an octocopter $r_1$=$lon_1$ vehicle sweep command will excite $lon_1$, $lon_2$, and $q$, with $lon_1$ and $lon_2$ being redundant control inputs and therefore completely correlated.

The second step is to extract the bare airframe frequency responses using the JIO method. In this case, the sweep commands are the references $\boldsymbol{r}$, the actuator signals in the JIO method are the summed actuators $\boldsymbol{\delta}_A = \boldsymbol{\delta}_{Sum}$ as shown in Fig. 2b, and the outputs any desired vehicle responses $\boldsymbol{y}$. For the

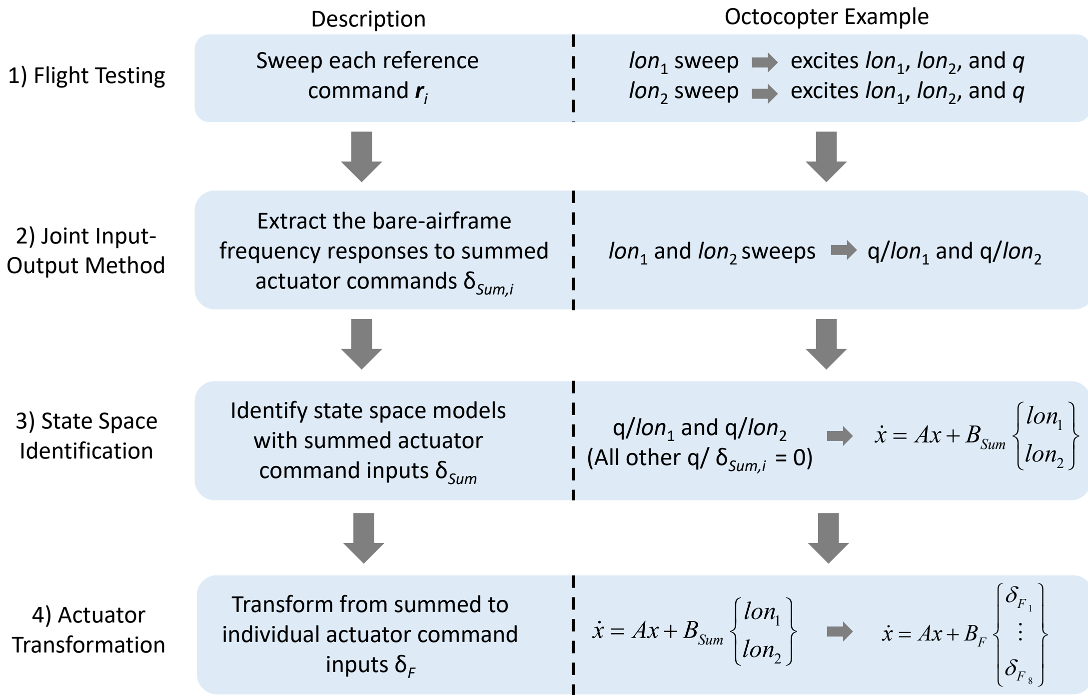


Fig. 5: Process for obtaining models with individual actuator commands.

octocopter pitch example, $r_1 = lon_1$ and $r_2 = lon_2$ sweeps are used to extract frequency responses $q/lon_1$ and $q/lon_2$. It should be noted that the choice of references and summed actuator commands results in all axes (heave, roll, pitch, and yaw) being mutually decoupled (e.g. for the octocopter, only $lon_1$ and $lon_2$ will cause any pitch rate response.

The third step is then to identify state space models with respect to the summed actuator command inputs. Once this appropriate frequency responses have been obtained throught the Joint-Input Output method, this state space identification is straightforward and follows the standard identification procedure (Ref. 4). Guidelines from Tischler are used for parameter reliability and model acceptability (Ref. 4). Cramér-Rao bounds are within 20% and insensitivities are within 10% for all identified parameters indicating good reliaibility. Table 2 shows the average and maximum cost functions for each configuration. All models have average cost functions $J_{ave} < 50$ (Ref. 4), indicating that overall each individual model is an excellent fit to its corresponding flight data. Maximum cost functions are also displayed for each configuration and are all below 100, indicating good levels of fit for corresponding frequency responses from flight data.

Table 2: Cost Functions for Identified State Space Models.

| Configuration | Average Cost Function | Maximum Cost Function |
|---|---|---|
| Quadcopter | 40.8 | 89.9 ($q/lon$) |
| Hexacopter | 45.5 | 98.4 ($\dot{u}/lon$) |
| Octocopter | 27.5 | 61.2 ($\dot{u}/lon$) |

It should be noted that there are 3 caveats for the state space identification, which are specific to the goal of the reconfigurable multicopter model. 1) All longitudinal and lateral derivatives are constrained to be equal after accounting for differences in inertia. 2) All actuator dynamics and delays are constrained to be equal. 3) Quad, hexa, and octocopter state space models all have the same structure. Each of the constraints are assumptions based on the symmetry of the vehicles and common parts used for each rotor and each vehicle. One consequence of these caveats is that the state space identification must be performed with all axes simultaneously; even though the vehicle dynamics are decoupled, the way to enforce symmetries among the axes and motors is by simultaenously identifying all axes with the inter-axis constsraints.

The final step is to transform the state space inputs from summed actuator commands to individual actuator commands. This is straightforward as the mixing matrix $\boldsymbol{M}$ was chosen to be invertible. A similar process is done to the states corresponding to actuator dynamics (motor lags), which is possible due to the constraint that all actuators are the same.

This process for identifying state space models with individual actuator command inputs is repeated for the quad, hexa, and octocopter. The final state space form is shown in Fig. 6 with individual actuator command inputs. The mass and inertia terms are explicity separated from aerodynamic terms in the stability and control matrices for the purposes of the reconfigurable model. All 3 configurations share the same state space form. The stability derivatives $X_w, Y_r, Z_u, Z_q, L_r, M_w, N_v$, and $N_p$ are all fixed to 0 due to their corresponding frequency responses being dropped as a result of the decoupled responses (Ref. 4). Additionally, the stability derivatives $X_q$

Mass and Inertias — Rigid Body Stability Derivatives — Control Derivatives — Motor Lags

$$
\begin{bmatrix}
m & 0 & 0 & 0 & 0 & 0 & 0 & 0 & 0 & 0 & 0 & \cdots & 0\\
0 & m & 0 & 0 & 0 & 0 & 0 & 0 & 0 & 0 & 0 & \cdots & 0\\
0 & 0 & m & 0 & 0 & 0 & 0 & 0 & 0 & 0 & 0 & \cdots & 0\\
0 & 0 & 0 & I_{xx} & 0 & 0 & 0 & 0 & 0 & 0 & 0 & \cdots & 0\\
0 & 0 & 0 & 0 & I_{yy} & 0 & 0 & 0 & 0 & 0 & 0 & \cdots & 0\\
0 & 0 & 0 & 0 & 0 & I_{zz} & 0 & 0 & 0 & 0 & 0 & \cdots & 0\\
0 & 0 & 0 & 0 & 0 & 0 & 1 & 0 & 0 & 0 & 0 & \cdots & 0\\
0 & 0 & 0 & 0 & 0 & 0 & 0 & 1 & 0 & 0 & 0 & \cdots & 0\\
0 & 0 & 0 & 0 & 0 & 0 & 0 & 0 & 1 & 0 & 0 & \cdots & 0\\
0 & 0 & 0 & 0 & 0 & 0 & 0 & 0 & 0 & 1 & 0 & \cdots & 0\\
0 & 0 & 0 & 0 & 0 & 0 & 0 & 0 & 0 & 0 & 1 & \cdots & 0\\
\vdots & \vdots & \vdots & \vdots & \vdots & \vdots & \vdots & \vdots & \vdots & \vdots & \vdots & \ddots & \vdots\\
0 & 0 & 0 & 0 & 0 & 0 & 0 & 0 & 0 & 0 & 0 & \cdots & 1
\end{bmatrix}
\begin{bmatrix}
\dot{u}\\ \dot{v}\\ \dot{w}\\ \dot{p}\\ \dot{q}\\ \dot{r}\\ \dot{\phi}\\ \dot{\theta}\\ \dot{\psi}\\ \dot{m}_1\\ \dot{m}_2\\ \vdots\\ \dot{m}_n
\end{bmatrix}
=
\left[\begin{array}{ccccccccc|cccc}
X_u & 0 & X_w & 0 & X_q & 0 & 0 & -mg\cos(\theta_e) & 0 & 0 & 0 & \cdots & 0\\
0 & Y_v & 0 & Y_p & 0 & Y_r & mg\cos(\theta_e) & 0 & 0 & 0 & 0 & \cdots & 0\\
Z_u & 0 & Z_w & 0 & Z_q & 0 & 0 & -mg\sin(\theta_e) & 0 & Z_{m_1} & Z_{m_2} & \cdots & Z_{m_n}\\
0 & L_v & 0 & L_p & 0 & L_r & 0 & 0 & 0 & L_{m_1} & L_{m_2} & \cdots & L_{m_n}\\
M_u & 0 & M_w & 0 & M_q & 0 & 0 & 0 & 0 & M_{m_1} & M_{m_2} & \cdots & M_{m_n}\\
0 & N_v & 0 & N_p & 0 & N_r & 0 & 0 & 0 & N_{m_1} & N_{m_2} & \cdots & N_{m_n}\\
0 & 0 & 0 & 1 & 0 & 0 & 0 & 0 & 0 & 0 & 0 & \cdots & 0\\
0 & 0 & 0 & 0 & 1 & 0 & 0 & 0 & 0 & 0 & 0 & \cdots & 0\\
0 & 0 & 0 & 0 & 0 & \sec(\gamma_e) & 0 & 0 & 0 & 0 & 0 & \cdots & 0\\
\hline
0 & 0 & 0 & 0 & 0 & 0 & 0 & 0 & 0 & -\omega_{m_1} & 0 & \cdots & 0\\
0 & 0 & 0 & 0 & 0 & 0 & 0 & 0 & 0 & 0 & -\omega_{m_2} & \cdots & 0\\
\vdots & \vdots & \vdots & \vdots & \vdots & \vdots & \vdots & \vdots & \vdots & \vdots & \vdots & \ddots & \vdots\\
0 & 0 & 0 & 0 & 0 & 0 & 0 & 0 & 0 & 0 & 0 & \cdots & -\omega_{m_n}
\end{array}\right]
\begin{bmatrix}
u\\ v\\ w\\ p\\ q\\ r\\ \phi\\ \theta\\ \psi\\ m_1\\ m_2\\ \vdots\\ m_n
\end{bmatrix}
+
\begin{bmatrix}
0 & 0 & \cdots & 0\\
0 & 0 & \cdots & 0\\
0 & 0 & \cdots & 0\\
0 & 0 & \cdots & 0\\
0 & 0 & \cdots & 0\\
N_{f_1} & N_{f_2} & \cdots & N_{f_n}\\
0 & 0 & \cdots & 0\\
0 & 0 & \cdots & 0\\
0 & 0 & \cdots & 0\\
\omega_{m_1} & 0 & \cdots & 0\\
0 & \omega_{m_2} & \cdots & 0\\
\vdots & \vdots & \ddots & \vdots\\
0 & 0 & \cdots & \omega_{m_n}
\end{bmatrix}
\begin{bmatrix}
f_1(t-\tau_1)\\ f_2(t-\tau_2)\\ \vdots\\ f_n(t-\tau_n)
\end{bmatrix}
$$

Fig. 6: State space model with individual actuator commands.

and $Y_p$ are fixed to 0 as they were found to be insenstive for all 3 vehicles. Additionally, the stability derivative $N_r$ is fixed to 0 for the quad and hexacopter configurations, as it was insensitve for those configurations. A final note is that there are motor lags present to account for motor dynamics; this is similar to previous work that found actuator dynamics were needed for other multicopter configurations (Ref. 6).

## RECONFIGURABLE MULTICOPTER MODEL

The reconfigurable multicopter model is derived from quad and octocopter flight identified models. The hexacopter configuration was also flight tested and a model was extracted, however this data was only used in validation of the reconfigurable model, not in the model development. The reconfigurable model is developed by producing a fit between each individual state space term of the quad and octocopter identified models.

Linear least squares fits are used for terms which are expected to vary linearly with the number of rotors or rotor placement. For example, mass varies linearly with the number of rotors, while inertias vary linearly with the rotor placement. It should be noted that inertias from identified models are computed from a spreasdsheet buildup of individual components and are fixed in the actual state space identification process. Figure 7 shows the pitch inertia for the reconfigurable model along with the values used in system identified models. The dashed line indicates the fit used in the reconfigurable model (RM Fit). The red “x”, black upward facing triangle, and blue circle indicate the pitch inertia for the quad, hexa, and octocopter respectively based on values used in the system identified models (based on a spreadsheet buildup). The downward facing magenta triangle indicates the pitch inertia for the hexacopter based on the reconfigurable model (Hexa RM). The reconfigurable model precisely predicts the hexacopter pitch inertia computed from a spreadsheet buildup as the Hexa RM and Hexa ID markers lie directly on top of one another.

The reconfigurable multicopter model is based on fits of the “basic derivatives” as defined by McRuer (Ref. 14). The

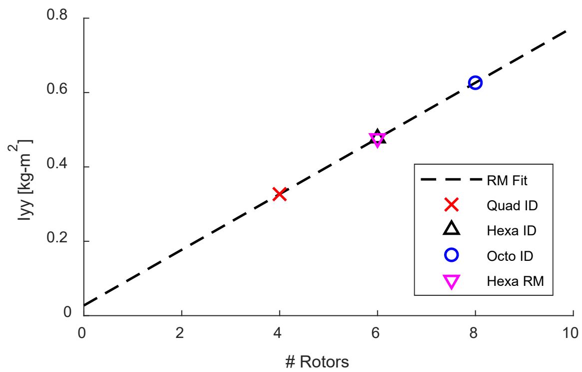


Fig. 7: Pitch inertia for reconfigurable model.

basic stability and control derivatives are in terms of force or moment, for example the basic pitch damping derivative has units of $[(Nm)/(rad/s)]$. This is in contrast to standard dimensional derivatives, which are in terms of acceleration, for example the standard dimensional pitch damping derivative has units of $[(rad/s^2)/(rad/s)] = [1/s]$. For clarity, the standard dimensional derivatives can be obtained by dividing the basic derivatives with the appropriate mass or inertia term. For example, standard dimensional pitch damping is obtained by dividing basic pitch damping by pitch inertia: $M_{q,dimensional} = M_{q,basic}/I_{yy}$. The standard dimensional derivatives are normally used in state space flight dynamic model identification. The basic derivatives are independent of mass and inertia, and are used in the reconfigurable model in order to separate the effects of inertia from aerodynamic effects.

Aerodynamic terms such as heave, roll, and pitch damping vary linearly with the number of rotors or rotor placement and are fit using linear least squares fits. Figure 8 shows the basic pitch damping derivative for the reconfigurable model along with values from system identified models. Error bars are shown indicating a 1-standard deviation confidence based on Cramér-Rao bounds. The reconfigurable model has an overall linear trend with the number of rotors as depicted in Fig. 8. The reconfigurable model accurately predicts the hexacopter

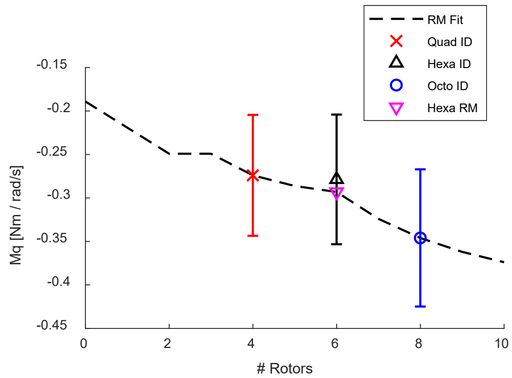


Fig. 8: Pitch damping for reconfigurable model (basic deriative).

basic pitch damping from the flight identified value, as the Hexa RM marker is very close to the Hexa ID marker, and well within the Hexa ID error bounds.

Step function fits are used for terms which do not vary linearly with the number of rotors, for example control derivatives are greatly affected by interference effects, which are a nonlinear function of rotor spacing. Figure 9 shows the basic pitch control derivative for an individual motor, relocated to be 1 meter from the vehicle center of gravity. Basic control power for an individual motor is shown in terms of moment [Nm] per motor input command [PWM]. For configurations where the number of rotors is less than 8, each motor has the same control power as an individual motor from the quadcopter. For configurations where the number of rotors is 8 or more, each motor has the same control power as an individual motor from the octocopter. Figure 9 shows a reduction in inidivdual motor control power between when the number of rotors is increased from 6 to 8. This reduction in individual motor control power is due to the decrease in rotor spacing resulting in rotors becoming physically close enough that significant aerodynamic interference occurs.

After accounting for the step function in individual motor control power and also accouting for changes in rotor placement and inertia, the total dimensional pitch control power for the reconfigurable model is shown in Fig. 10. Total dimensional control power is shown in terms of vehicle angular acceleration [rad/s$^2$] per mixer input command [PWM]. Due to all factors combined (aerodynamic interference and changes in rotor placement and inertia), the quadcopter vehicle acutally has the largest total dimensional control power in pitch. Compared to the quadcopter, the hexacopter has significantly less total pitch control power. The octocopter has more total pitch control power compared to the hexacopter, but not as much as the quadcopter. Thus, adding more rotors can result in a net increase or decrease in total control power, which may contradict initial intuition.

Similar validations for all individual state space terms (Fig. 6) were performed between the hexacopter directly identified model and the hexacopter configuration from the reconfigurable model. All terms from the reconfigurable model based hexacopter were within the 1-standard deviation error bounds from the directly identified hexacopter model, validating that the reconfigurable model is able to predict individual terms within the accuracy of the directly identified hexacopter model.

## FLIGHT DATA VALIDATION

After the reconfigurable model has been validated at the hexacopter flight identified configuration for all state space model terms, it is next checked against the identified hexacopter in comparison to the actual flight data using frequency responses.

Figure 11 shows the pitch rate response due to a longitudinal mixer input for flight data, state space model directly identified from flight data (Hexacopter ID), and state space model from the reconfigurable model (Hexacopter RM). The directly identified and reconfigurable model responses lie directly on top of each other, both with nearly identical costs (J = 73 vs 75). This shows that the reconfigurable model is able to predict the pitch rate response just as well as the directly identified hexacopter model.

The costs for all frequency responses are compared for the reconfigurable model and the directly identified hexacopter model in Table 3. The Hexa ID column is the cost of the directly identified state space model compared to the flight data. The Hexa RM column is the cost of the reconfigurable model compared to the hexacopter flight data. For all frequency responses, the reconfigurable model has a cost similar to the directly identified model. On average, the reconfigurable model has a cost of 46.0 which closely compares to the average directly identified model cost of 45.5, meaning that the reconfigurable model is able to predict flight data frequency responses just as well as the directly identified hexacopter model.

Table 3: Cost Functions for Hexacopter Identified and Reconfigurable Models.

| Response | Hexa ID | Hexa RM |
|---|---|---|
| $a_z/col_1$ | 13.6 | 13.6 |
| $a_z/col_2$ | 60.7 | 56.6 |
| $a_z/col_3$ | 79.4 | 83.9 |
| $\dot{u}/lon$ | 98.4 | 97.8 |
| $q/lon$ | 73.3 | 75.1 |
| $a_x/lon$ | 45.3 | 49.3 |
| $\dot{v}/lat$ | 27.2 | 27.2 |
| $p/lat$ | 23.9 | 23.8 |
| $a_y/lat$ | 28.3 | 26.8 |
| $r/ped$ | 5.4 | 5.4 |
| Average | 45.5 | 46.0 |

The reconfigurable model and directly identified hexacopter model are checked in the time domain with doublet response flight data. Figure 12 shows the pitch rate response due to a longitudinal doublet for flight data, state space model directly identified from flight data (Hexacopter ID), and state space

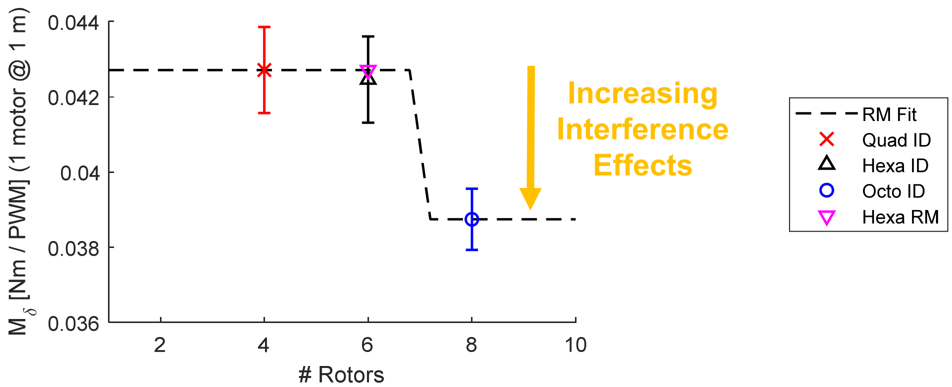


Fig. 9: Pitch control power for an individual motor (basic derivative).

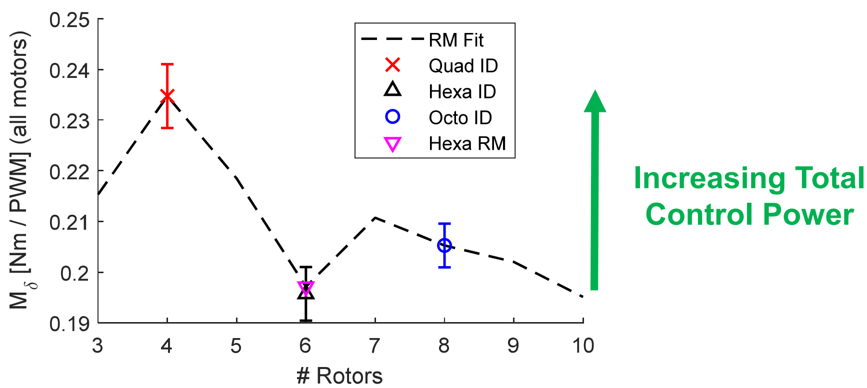


Fig. 10: Total pitch control power for reconfigurable model (dimensional derivative).

model from the reconfigurable model (Hexacopter RM). The directly identified and reconfigurable model responses lie directly on top of each other.

The RMS cost of the time response data can be Froude scaled based on multicopter hub-to-hub distance scaled to UH-60 rotor diameter to so that existing RMS cost guidelines can be applied (Ref. 4). Both models have the same scaled RMS cost $J_{RMS,Scaled} = 0.78 < 2$, and both models have a Theil Inequality Coefficient $TIC = 0.08 < 0.3$. This shows that the reconfigurable model is able to predict the pitch rate response in the time domain just as well as the directly identified hexacopter model, and both are extremely accurate (Ref. 4).

The $J_{RMS,Scaled}$ and $TIC$ values for all axes are shown in Table 4. The ID columns are the scaled RMS cost and TIC of the directly identified state space model compared to the flight data. The RM columns are the scaled RMS cost and TIC of the reconfigurable model compared to the hexacopter flight data. For all doublet responses, the reconfigurable model has a cost and TIC similar to the directly identified model. On average, the reconfigurable model has an RMS cost $J_{RMS,Scaled} = 0.73$ and $TIC = 0.13$ which closely compares to the average directly identified model $J_{RMS,Scaled} = 0.70$ and $TIC = 0.11$, meaning that the reconfigurable model is able to predict flight data frequency responses just as well as the directly identified hexacopter model.

Table 4: Scaled RMS Cost and Thiel Inequality Coefficients for doublet verification.

| Input | ID Cost | RM Cost | ID TIC | RM TIC |
|---|---|---|---|---|
| $col_{mixer}$ | 0.43 | 0.55 | 0.07 | 0.09 |
| $lon_{mixer}$ | 0.79 | 0.79 | 0.08 | 0.08 |
| $lat_{mixer}$ | 1.28 | 1.28 | 0.16 | 0.16 |
| $ped_{mixer}$ | 0.31 | 0.31 | 0.17 | 0.18 |
| Average | 0.70 | 0.73 | 0.11 | 0.13 |

## CONCLUSIONS

To study the inherent effects of the number of rotors on gust rejection capability, a quad, hexa, and octocopter were built and used to obtain system identified flight dynamics models. The quad and octocopter configurations were then used to develop a reconfigurable multicopter model, which was validated with hexacopter flight data and a directly identified model. This work supports the following conclusions:

1. Frequency response system identification augmented with the Joint Input-Output method can be used to extract stability and control contributions from individual rotors of a multicopter vehicle.

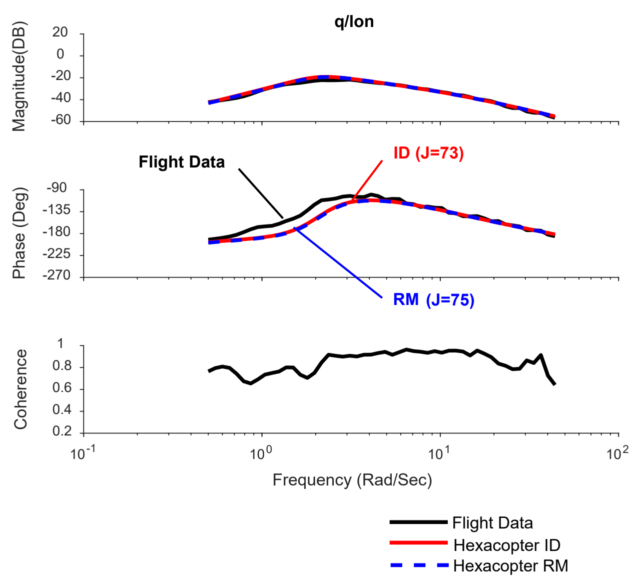


Fig. 11: Pitch rate response to longitudinal mixer input.

2. A reconfigurable multicopter model based on identified quad and octocopter configurations can be used to predict hexacopter flight dynamics parameters and responses just as well as a directly identified model.

3. Individual rotor control power may be reduced when the number of rotors is increased. This is due to decreased rotor spacing which results in significant aerodynamic interference effects between rotors.

4. Increasing the number of rotors on a multicopter may not inherently add control power or gust rejection capability. Adding rotors affects inertia, rotor placement, and individual rotor control power and all 3 effects combined can result in an increase or decrease in total control power.

## ACKNOWLEDGMENTS

This work was sponsored by the Defense Advanced Research Project Agency, Tactical Technology Office (DARPA TTO) under the Gust Rejection effort at the Aviation Development Directorate (ADD) - Ames, managed by Dr. Alexander M. G. Walan. The authors would like to thank the Gust Rejection team at DARPA TTO for their support. The authors would also like to thank Dr. Mark F. Costello for his support of the gust rejection work at ADD.

## REFERENCES

[1]Bristeau, P., Martin P., Salaun, E., and Petit, N., "The Role of Propeller Aerodyanmics in the Model of a Quadrotor UAV", Proceeding of the European Control Conference 2009, Budapest, Hungary, August 23-26, 2009.

[2]Russel, C. R. and Sekula, M. K., "Comprehensive Analysis Modeling of Small-Scale UAS Rotors", presented at the AHS International 73rd Annual Forum & Technology Display, Fort Worth, TX, May 9-11, 2017.

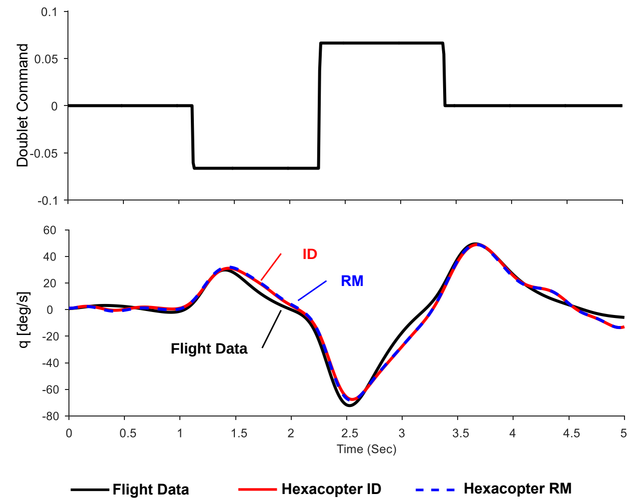


Fig. 12: Pitch rate response to doublet command.

[3]Niemiec, R., Gandhi, F., and Singh, R., "Control and Performance Analysis of a Reconfigurable Multi-Copter", presented at the AHS International 73rd Annual Forum & Technology Display, Fort Worth, TX, May 9-11, 2017.

[4]Tischler, M. B. and Remple, R. K., *Aircraft and Rotorcraft System Identification: Engineering Methods with Flight Test Examples*, 2nd Edition, American Institute of Aeronautics and Astronautics, Inc., Reston, VA, 2012.

[5]Wei, W., Cohen, K., and Tischler, M. B., "System Identification and Controller Optimization of a Quadrotor UAV", presented at the AHS 71st Annual Forum, virginia beach, VA, May 5-7, 2015.

[6]Juhasz, O., Lopez, M. J. S., Berrios, M. G., Berger, T., and Tischler, M. B., "Turbulence Modeling of a Small Quadrotor UAS Using System Identification from Flight Data", presented at the Seventh AHS Technical Meeting on VTOL Unmanned Aircraft Systems, Mesa, AZ, January 24-26, 2017.

[7]Berrios, M. G., Berger, T., Tischler, M. B., Juhasz, O., and Sanders, F. C., "Hover Flight Control Design for UAS Using Performance-based Disturbance Rejection Requirements", presented at the AHS International 73rd Annual Forum & Technology Display, Fort Worth, TX, May 9-11, 2017.

[8]Akaike, H., "Some Problems in the Application of the Cross-Spectral Method," Spectral Analysis of Time Series, edited by B. Harris, Wiley, New York, 1967, pp.81-107.

[9]Gennaretti, M., Gori, R., Serafini, J., Cardito, F., and Bernardini, G., "Identification of Rotor Wake Inflow Finite-State Models for Flight Dynamics Simulations," CEAS Aeronautical Journal, Vol. 8, No. 1, 2017, pp. 209230.

[10]Hersey, S., Celi, R., Juhasz, O., Tischler, M. B., Rand, O., and Khromov, V., "State-Space Inflow Model Identification and Flight Dynamics Coupling for an Advanced Coaxial Rotorcraft Configuration" , presented at the AHS International

73rd Annual Forum & Technology Display, Fort Worth, TX, May 9-11, 2017.

[11]Knapp, M. E., Berger, T., Tischler, M. B., and Cotting, M. C., "Development of a Full Envelope Flight Identified F-16 Simulation Model", AIAA Paper 2018-0525, 2018.

[12]Berger, T., Tischler, M. B., Knapp, M. E., and Lopez, M. J. S., "Identification of Multi-Input System in the Prescence of Highly Correlated Input", AIAA Journal of Guidance, Control, and Dynamics, June 27, 2018.

[13]Berger, T., Tischler, M. B., Knapp, M. E., and Lopez, M. J. S., "Identification of Multi-Input System in the Prescence of Highly Correlated Inputs", presented at the Atmospheric Flight Mechanics Conference at AIAA SciTech, San Diego, CA, January 7-11, 2019.

[14]McRuer, D. T., Graham, D., and Ashkenas, I., *Aircraft Dynamics and Automatic Control*, Princeton University Press, Princeton, NJ, 1973.